Available online at www.sciencedirect.com
ScienceDirect
Journal of the European Ceramic Society 29 (2009) 1093–1099
www.elsevier.com/locate/jeurceramsoc

# Microstraining in titania-, alumina- and silica-supported $V_2O_5$-catalysts

D. Habel [a,*], O. Görke [a], M. Tovar [b], M. Willinger [c], M. Ziemann [a], O. Schwarz [d], R. Schomäcker [d], H. Schubert [a]

[a] *TU Berlin, Institute of Material Science and Technologies, Englische Straße 20, D-10587 Berlin, Germany*
[b] *Hahn-Meitner-Institute, Division of Structure Research, Glienicker Straße 100, D-14109 Berlin, Germany*
[c] *Fritz-Haber-Institute of the Max Planck Society, Department of Inorganic Chemistry, Faradayweg 4-6, D-14195 Berlin, Germany*
[d] *TU Berlin, Institute for Chemistry, Str. des 17. Juni 124-128, D-10623 Berlin, Germany*

Received 9 February 2008; received in revised form 25 July 2008; accepted 31 July 2008
Available online 30 December 2008

**Abstract**

Commonly used catalysts in industry are compositions of highly dispersed particles. Typical systems consist of precious metals or transition metal oxides like $V_2O_5$ on oxide supports, especially $TiO_2$, $Al_2O_3$ and $SiO_2$. Support and active compound show a different chemical and material behaviour. A very important influence of the support on the active compound is the formation of microstrains due to the different thermal expansion behaviour. On the surface of a stiff linear elastic support the active compound is certainly strain hindered. In order to monitor the development of strain hindrance and further effects, in situ experiments were carried out at temperature both in an X-ray and in a neutron powder diffractometer. The width of the reflexes indicated a strong influence of the thermal expansion mismatch on peak width. The strain hindrance creates mismatch stresses high enough to overcome the yield stress of $V_2O_5$. The Williamson–Hall plots showed both a particle size effect as well as a stress widening but the measurements were difficult because of the materials anisotropy. The TEM work showed again very fine particles which agrees with the X-ray measurements. The support effect may be seen as thermal stress induced formation of a mosaic structure in the active compound. Moreover, the peak width correlated with the catalytic activity. The low ordered regimes in the mosaic structure are acting as further active centres for the catalytic reaction.


*Keywords:* Microstructure-final; X-ray methods; Thermal expansion; $TiO_2$; $V_2O_5$

## 1. Introduction

The dehydrogenation of olefins is a key step in chemical industry.[1–4] The ODP reaction (oxidative dehydrogenation of propane) may be seen as one model reaction for olefin processing to produce propene at low temperatures. The reaction requires a contact of the gas molecule to solid-state catalyst which donates oxygen to react with two hydrogen species of the gas. This mechanism was described by Mars and van Krevelen.[5] The first products are propene and water as an off product. Propene can undergo a total combustion to CO and $CO_2$. It has been found that vanadium based systems are appropriate catalysts for the oxidative dehydrogenation of propane.[6–10] $TiO_2$ has been intensively investigated as a support (Eurocat).[11–15] The existence of different surface vanadium oxides on various supports has been the subject of several studies.[9,16–21]

A classical preparation process in chemical industry is to mill both support and active compound added as oxides. The slurries are then typically spray dried to produce large-scale granules with adequate strength to serve in a powder bed reactor. Thus this work is focussed to inspect the role of the support crystalline particles of sizes in 100 nm range with an amount in the percent range. It has been shown that the support alters the active compound even if it occurs as crystalline particles in fairly high amounts. In spite of the quite large size (100 nm ≈ 100 unit cells) the support is able to change the activity of the active compound.

For this work three different supports ($Al_2O_3$, $TiO_2$ and $SiO_2$) have been chosen which differ with respect to physical properties from which the thermal expansion behaviour is considered to have dominating influence. The thermal expansion coefficients for the support materials have been reliably reported by

* Corresponding author. Tel.: +49 30 314 249 76; fax: +49 30 314 240 72.
*E-mail address:* habel@ms.tu-berlin.de (D. Habel).

0955-2219/$ – see front matter © 2008 Elsevier Ltd. All rights reserved.
doi:10.1016/j.jeurceramsoc.2008.07.065

Touloukian[22] but the values for the highly anisotropic layered structure of $V_2O_5$ were uncertain and had to be measured.

Thermal stresses arising from a thermal mismatch between the support and the active compound are a function of the elastic moduli, of the thermal mismatch and the temperature change. Residual stresses are elastic stresses that remain in a body after all external loads have been removed. Residual stresses build up in the catalyst during cooling from processing temperature to room temperature or during service.

X-ray diffraction techniques can be used to measure residual stresses. The crystal lattice is used as a strain gage. The basic principle is that the presence of a residual stress will change the interplanar spacings of the lattice planes and thus cause a shift in the diffraction peaks. The strains are measured directly and the stresses are obtained through appropriate elastic constants.

This paper focussed on investigations due to the role of the different expansion behaviour on the alteration of the active compound, the investigation of microstrains resulting in a mosaic structure and the impact on catalytic activity.

## 2. Experimental

The materials have been prepared by standard ball milling of $TiO_2$ (Anatase modification, GL 102/10827, KRONOS International Inc., Germany, $d_{50} = 0.54\ \mu m$), $Al_2O_3$ (α-alumina, AKP 50, Sumimoto, Japan, $d_{50} = 0.68\ \mu m$) and $SiO_2$ (Cristobalite, Sikron 6000, Quarzwerke Frechen, Germany, $d_{50} = 3.71\ \mu m$) as supports as well as $V_2O_5$ as active compound (Shcherbinaite modification, GfE Environmental Technology Ltd., Germany, $d_{50} = 1.65\ \mu m$) in dried cyclohexane for 1 h (SiC milling balls, PE lining). The mixed powders were dried at 100 °C and sieve granulated. Alternatively, the active compound was introduced as a soluble vanadylisopropylate precursor which could be hydrolyzed easily. A stable interface was established by heating 500 °C in air (Nabertherm Lilienthal, Germany) for 2 h. The heating rate was −270.15 °C/min.

The XRD work requires different scattering geometries. For the phase analysis a Bruker D5005 diffractometer (Karlsruhe, Germany) with a position sensitive detector was used ($\theta - \theta$) for wide range scans (step width 0.008° 2$\theta$, Cu Kα radiation). A Bruker diffractometer D5000 ($\theta - 2\theta$) in Bragg–Brentano geometry with a Buehler heating chamber (PT-resistance heater) and a scintillation counter enabled measurements at various temperatures and partial pressures. All measurements were performed with an internal 8Y-CSZ standard (Tosoh, Japan).

The Fourier program "Profile" (Bruker AXS) run based on a Pseudo Voigt function to deconvolut the peaks and to determine the peak width.

The TEM images were carried out using a Philips CM 200 FEG with a Catan detector in transmission geometry. Images were modified with colours with the Digital Micrograph program.

Catalytic tests of $V_2O_5$ on different oxidic supports were carried out in packed bed tubular reactors using the oxidative dehydrogenation of propane (ODP) as test reaction. The applied gas mixture was composed of 40 vol.% $C_3H_8$:20 vol.% $O_2$:40 vol.% Ne. All the tests were carried out at 500 °C.

## 3. Results and discussion

### 3.1. Thermal expansion

The crystallographic structures of the support materials are different but they differ even more from the active compound. The thermal expansion coefficients of the support materials are well described in the Handbook of Touloukian.[22] $Al_2O_3$ ($\alpha = 8.0 \times 10^{-6}\ K^{-1}$) and $TiO_2$ ($\alpha = 9.0 \times 10^{-6}\ K^{-1}$) have similar thermal expansion coefficients, whereas the value for $SiO_2$ ($\alpha = 0.5 \times 10^{-6}\ K^{-1}$) is much lower.

There are only two sources for $V_2O_5$ data which are indicating a pronounced anisotropy but their values do not entirely coincide.[23,24] Since axial thermal expansion coefficients are gained from a small variation of lattice constants accurate measurements were needed. Thus high temperature neutron diffraction experiments were carried out at E9 diffractometer at HMI (BENSC Berlin Neutron Scattering Center) in Berlin. The lattice constants at temperatures up to 500 °C were compared to those at room temperature to determine the linear thermal expansion coefficients using

$$\frac{a_T - a_{RT}}{a_{RT}} = \varepsilon_a = \alpha_a \times T$$

and analogously $\alpha_b$ and $\alpha_c$ from the changes in lattice parameters $b$ and $c$. The measured lattice constants and the expansion coefficients of $V_2O_5$ are given in Table 1.

$V_2O_5$ shows a layered orthorhombic structure with $a$–$b$ plane with high binding strength but lower binding strength in the $c$-axis. The structure is highly anisotropic. The strength of the material is very small, even touching particles of solidified melt droplets led to instantaneous cracking. The data reflect the anisotropy of the structure. The thermal expansion of the $c$-axis is extraordinary high while the coefficient for the $a$-axis is in a common range. The value for the $b$-axis is small and positive. Thus the material shows a normal expansion in two axes and a very high one in the third. So a highly anisotropic thermal mismatch between active compound and support can be expected.

### 3.2. High temperature X-ray diffraction

In order to monitor the development of strain hindrance and further effects, in situ investigations in a HT-XRD experimental setup were performed. The heater was a current heated Pt-foil loaded with pure $V_2O_5$ or mixed powders of $V_2O_5$ or $V_2O_3$ on distinct oxidic supports. Fig. 1 shows the peak widths (FWHM) of the $V_2O_5$ ⟨0 0 1⟩ reflex and the $V_2O_3$ ⟨1 0 4⟩ reflex for different powder samples treated under real catalytic feedgas or synthetic air.

The straining is represented by peak widening. The peak width of the starting material is broadened and reflects the previous milling action (column 1 in Fig. 1). Reaching the 500 °C the peak positions are shifted due to the thermal expansion. More important, the peak width at 500 °C is comparably small (column 2 in Fig. 1). After a dwell time of 2 h both phases were equilibrated (column 3 in Fig. 1). Because of a temperature of

Table 1
Lattice constants and axial thermal expansion coefficients of $V_2O_5$.

| Temperature (°C) | *a*-Axis | *b*-Axis | *c*-Axis | $\alpha_a$ ($\times 10^{-6}$ K$^{-1}$) | $\alpha_b$ ($\times 10^{-6}$ K$^{-1}$) | $\alpha_c$ ($\times 10^{-6}$ K$^{-1}$) |
|---|---|---|---|---|---|---|
| RT | 11.49802 | 3.55862 | 4.36624 | | | |
| 400 | 11.52768 | 3.56397 | 4.45594 | | | |
| 500 | 11.53352 | 3.56297 | 4.47558 | 7 | 2 | 52 |

almost 83% of the melting point of $V_2O_5$ fast diffusion and no reason for strain hindrance can be estimated. The peak width (FWHM) is smallest at the end of the isothermal dwell time. During cooling the mismatch rise up and at room temperature a maximum peak width for the active compound occurred (column 5 in Fig. 1). This series of peak widths basically shows the importance of the strain hindrance due to the difference in thermal expansion behaviour of active compound and support (columns 1–5 in Fig. 1).

If different supports are used, different mismatch situations occur. This can be seen from the comparison of peak width for samples with 5 mol% $V_2O_5$ on a $TiO_2$-, $Al_2O_3$- and $SiO_2$-support heat treated in air (columns 6–8 in Fig. 1).

Catalysts in service are subject to reduction which is associated with phase changes. $V_2O_5$ reacts to $V_2O_3 + O_2$ under feedgas (40 vol.% $C_3H_8$:20 vol.% $O_2$:40 vol.% Ne) or 100 vol.% CO. The weight loss caused by oxygen loss is also associated with straining and leads to a further increase in peak width for the Karelianite ($V_2O_3$) 104 reflex on $TiO_2$, $Al_2O_3$ and $SiO_2$ (columns 9–11 in Fig. 1).

### 3.3. Reflex profiles

Since there are various reasons for peak widening a more detailed analysis was needed. The classical Warren–Averbach[26] method was reported for cubic materials, which is certainly not the case for highly anisotropic $V_2O_5$. Thus the Williamson–Hall plot was applied for $V_2O_5$ supported on $TiO_2$, $Al_2O_3$ and $SiO_2$ (Figs. 2 and 3). Microstrains and crystallite size can be determined with the Williamson–Hall method by plotting reciprocal peak widths versus reciprocal lattice distances. The evaluation of the changing peak widths of the active compound $V_2O_5$ was analysed with the reflexes of different lattice planes. Values for particle sizes and microstrains were obtained from the ordinate intercepts and the slopes, respectively, of straight lines.[27]

All support materials are characterized by a high elastic modulus and did not show much peak widening with almost no change with scattering angle. They do not suffer stresses and they do not have a too small crystallite size. This can be seen from the curves for the $Al_2O_3$ support in Fig. 2a. The values are small and there is no trend with scattering angle. In contrast the lines for the active compound $V_2O_5$ had high values and a strong decrease with scattering angle. The analysis was carried out using peaks given by the planes ⟨0 0 1⟩, ⟨1 0 1⟩, ⟨1 1 0⟩, ⟨0 1 1⟩, ⟨1 1 1⟩ and ⟨3 1 0⟩. This can be explained by small crystallite size ranging around 20 nm and stresses within the material, which

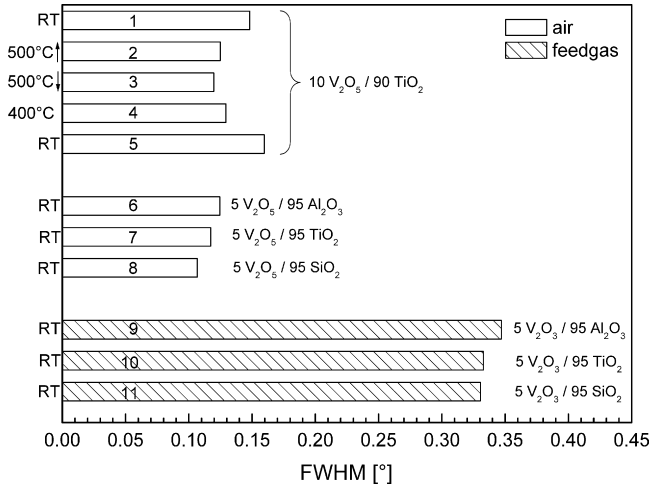


Fig. 1. Peak width (FWHM) of $V_2O_5$ ⟨0 0 1⟩ and $V_2O_3$ ⟨1 0 4⟩ reflexes for different samples and gas atmospheres.

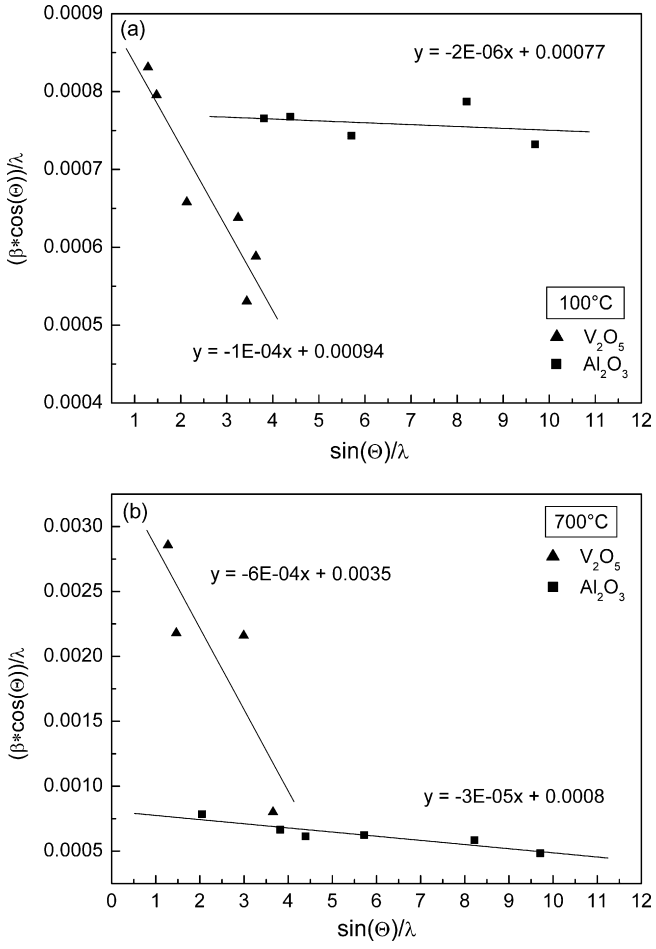


Fig. 2. Williamson–Hall plots for $V_2O_5/Al_2O_3$ annealed at 100 °C (a) and 700 °C (b).

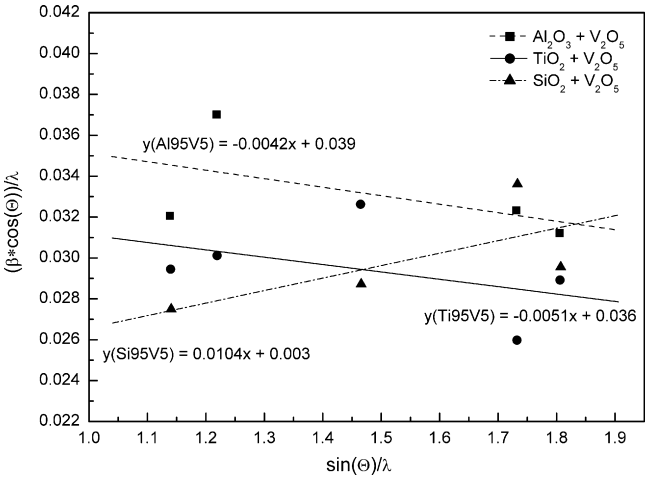


Fig. 3. Williamson–Hall plots for 5 mol% $V_2O_5$ on $Al_2O_3$-, $TiO_2$- and $SiO_2$-support annealed at 500 °C.

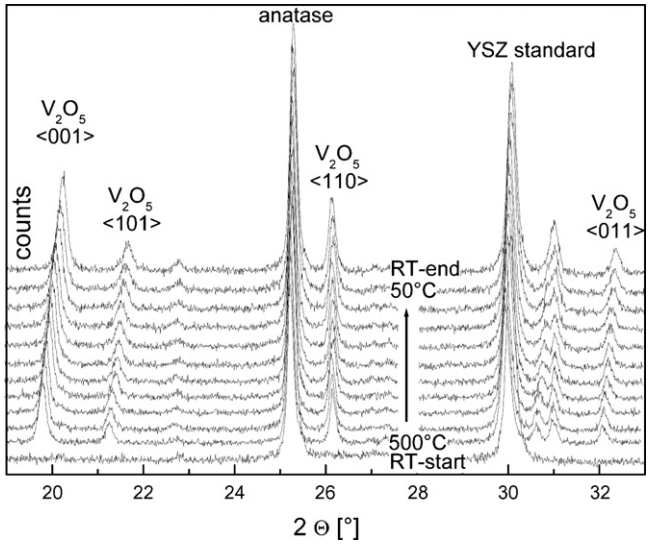


Fig. 4. X-ray diffractograms for a $V_2O_5$–$TiO_2$ specimen (vanadylisopropylate as precursor) for temperatures varying from 500 °C down to the room temperature in air (YSZ = yttria stabilized zirconia as standard).

are attributed to third-order stresses (microstresses). Furthermore, an influence of the temperature is conspicuous. Samples annealed at 700 °C show higher stresses than samples annealed at 100 °C (Fig. 2b). For this plot the $V_2O_5$ planes ⟨0 0 1⟩, ⟨1 0 1⟩, ⟨3 0 1⟩ and ⟨3 1 0⟩ were used.

$V_2O_5$ supported on $Al_2O_3$ and $TiO_2$ show related lines due to the similar thermal expansion coefficients of the supports. Otherwise the thermal expansion coefficient of the $SiO_2$ support is very small, thus the difference to the high thermal expansion coefficient of $V_2O_5$ causes higher stresses which can be seen as a higher slope of the curve (Fig. 3).

The data straggling of the Williamson–Hall analysis is quite high. Some of the assumptions of the theory do not apply. Especially, the assumption of a homogeneous stress field is critical. Nano particles of an anisotropic phase on the surface do not have a homogeneous stress distribution. For more accurate results the much more complex "Rietveld average particle size method" should be applied in the future.

### 3.4. Estimation of yield stresses

Since $V_2O_5$ is a highly anisotropic structure with respect to both thermal and elastic behaviour, the true load deflection behaviour is not known yet. If one assumes a simple linear elastic behaviour very high stresses should rise, which would be certainly higher than the strength of the material. The measurement of the peak width during cooling was carried out to monitor critical temperature, strain and finally stress (Figs. 4 and 5).

The peak profiles are comparably small at annealing temperature of 500 °C and become slightly wider on cooling (Fig. 4).

In Fig. 5 two regimes can be identified. For both $V_2O_5$ ⟨0 0 1⟩ and $V_2O_5$ ⟨1 1 0⟩ reflexes an increase in peak width is observed for temperatures smaller than 300 °C. Thus 300 °C is considered as a critical temperature. The microstructure appears to have thermal mismatch starting from 500 to 300 °C. Then the thermal stresses are high enough to overcome the yield stress. Knowing both the critical temperature and the thermal expansion coefficients of $V_2O_5$ and $TiO_2$ a difference in strain can be evaluated.

The thermal strain up to a temperature $T$ is

$$\Delta\varepsilon_{\mathrm{th}\,V_2O_5} = \alpha_{V_2O_5} \times \Delta T \quad \text{and}$$

$$\Delta\varepsilon_{\mathrm{th}\,TiO_2} = \alpha_{TiO_2} \times \Delta T, \quad \text{respectively.}$$

The resulting data for critical stresses in the active compound $V_2O_5$ are approximately 10 MPa and less when an estimated Youngs modulus of 10 GPa for $V_2O_5$ was used. This is in accordance to the known sensitivity of vanadia to any mechanical load. This estimation is not very accurate because of the number of assumptions. The differences between the low Youngs modulus of $V_2O_5$ and the Youngs modu-

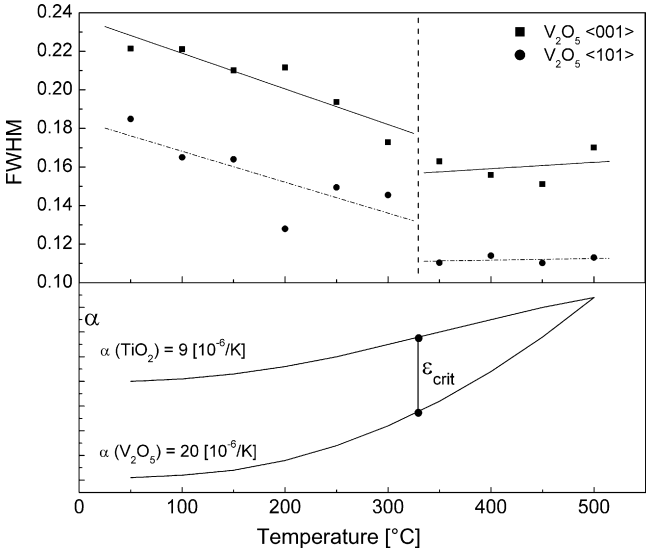


Fig. 5. Peak width of the $V_2O_5$ ⟨0 0 1⟩ and ⟨1 1 0⟩ reflexes (FWHM) for a $V_2O_5$–$TiO_2$ specimen (vanadylisopropylate as precursor) for temperatures varying from 500 °C down to the room temperature in air.

Table 2
Critical strain and yield stresses for the $V_2O_5$ *a*-, *b*- and *c*-axis.

| Axis | Strain $V_2O_5$ | Yield stress $V_2O_5/TiO_2$ (MPa) | Yield stress $V_2O_5/Al_2O_3$ (MPa) | Yield stress $V_2O_5/SiO_2$ (MPa) |
|---|---|---|---|---|
| *a* | 1.96E−3 | 5.6 | 2.8 | −18.2 |
| *b* | 5.60E−4 | 19.6 | 16.8 | −4.2 |
| *c* | 1.46E−2 | −120.4 | −123.2 | −144.2 |

lus of the applied supports ($E_{Al_2O_3}$ = 280–350 GPa, $E_{TiO_2}$ = 190–270 GPa, $E_{SiO_2}$ = 70–80 GPa) give an idea on the range of yield stress.[28] Table 2 summarizes the strains of $V_2O_5$ in its axes and the yield stresses for the samples with different oxidic supports.

### 3.5. TEM investigations

The difference in thermal expansion behaviour of strain hindered active compound particles leads to segmentation and the formation of a mosaic structure. The X-ray diffraction method has the advantage of a good statistical basis while TEM considers single particles. The TEM image in Fig. 6 shows a $V_2O_5$ particle at its interface to the $TiO_2$-support after annealing at 500 °C for 2 h.

The interface near region shows stress contrast while the outer region is less distorted. Fig. 6a shows dark contrasts and various lattice orientations in a $V_2O_5$ particle. The "Digital Micrograph" software enables to distinguish between the different crystallites with a homogeneous crystallographic orientation (Fig. 6b). Crystallites are very small and their size ranges from 5 nm to approximately 50 nm.

### 3.6. Development of the mosaic structure

The thermal history of the supported catalyst and the development of the microstructure may be seen as follows: both the support and the active compound are in equilibrium. $V_2O_5$ has a melting temperature of 658 °C, therefore, an annealing temperature of 500 °C is about 80% of the melting temperature, i.e. certainly high enough for grain boundary diffusion or even for volume diffusion. In such a temperature regime the phases relax any prior stresses and take their morphology. This process is driven by the minimization of enthalpy. Thus the size as detected by TEM is the primary result of the annealing temperature. On cooling both active compound and support are changing dimension due to their different thermal expansion behaviour. However, because both phases are bound by their interface the thermal strain cannot be relaxed by shape change. This strain hindrance raises mismatch stresses.

### 3.7. Correlation to catalysis

Two important characteristics of catalysis are the activity and the selectivity. The activity describes the propane conversion in dependence of the modified residence time which includes the amount of catalyst and gas flow. The selectivity describes the efficiency of the catalytic reaction by generating propene and unwanted by-products.

The results of the catalytic tests are given as activity and selectivity of supported $V_2O_5$ in Fig. 7.

The catalytic system with the $Al_2O_3$-support shows the highest activity but only average selectivity. The catalyst with

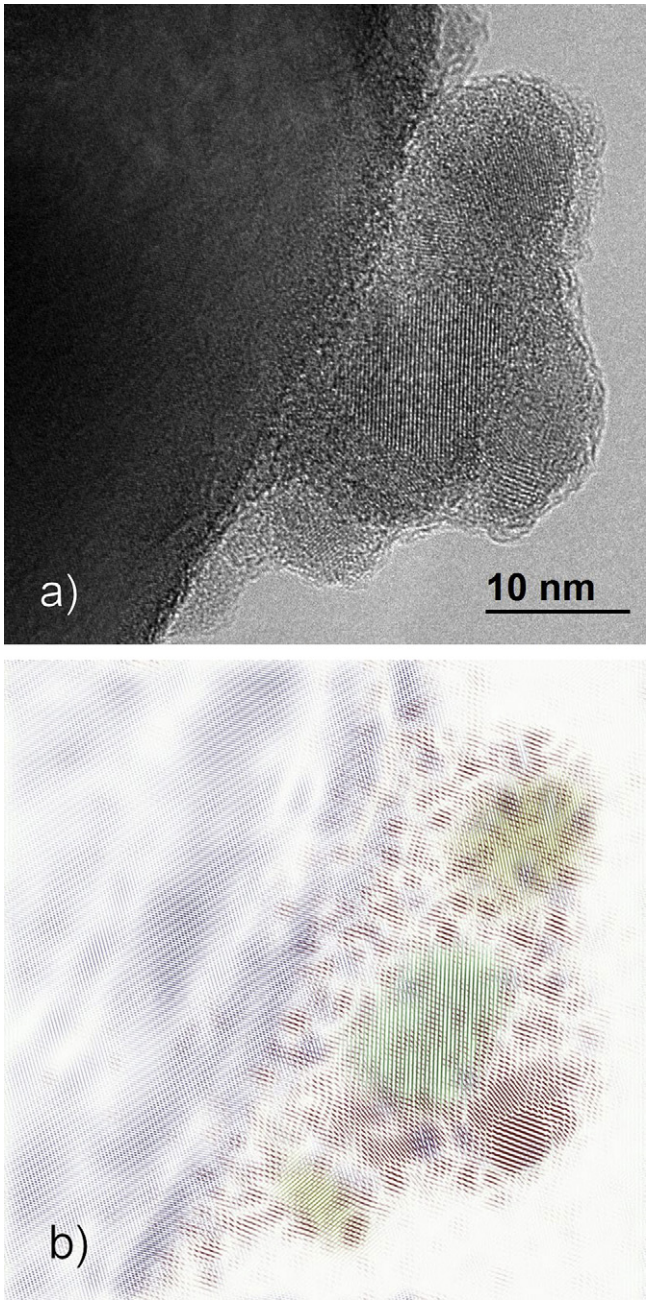


Fig. 6. TEM images of a $V_2O_5$ particle on a $TiO_2$-support; mosaic structure of $V_2O_5$ (a) and $V_2O_5$ with different crystallographic orientations (b).

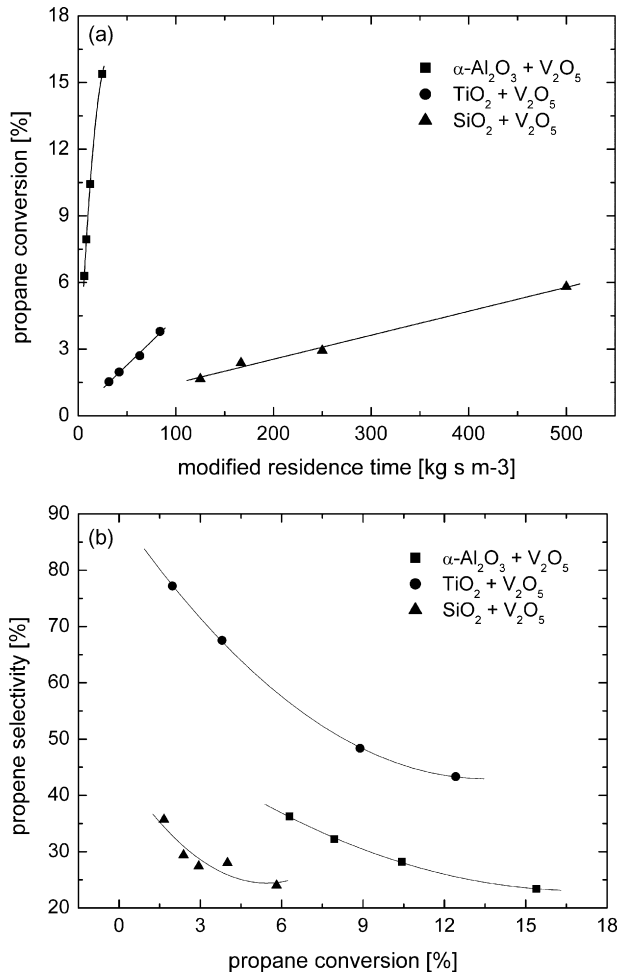


Fig. 7. (a) Activity of supported $V_2O_5$ (3 wt.%) catalysts. (b) Selectivity of supported $V_2O_5$ (3 wt.%) catalysts.

$TiO_2$-support reaches the best values for the selectivity. The worst performance for activity and selectivity is observed by the $SiO_2$-supported catalysts.

Furthermore, there is a proportionality of the activity and the peak width of different catalytic samples. Alumina supported $V_2O_5$ shows the highest activity and the highest peak width; silica supported $V_2O_5$ has the smallest values, respectively. This can be explained considering the mosaic structure. The real structure of the active compound is characterized by a high number of nano-sized domains which are separated by grain boundaries. The decrease in particle size and the increase in low coordinated sites (surface and grain boundaries) are attributed to an increase in the number of active sites and the increase in catalytic activity.

## 4. Summary

- $V_2O_5$ shows a significant anisotropy of thermal expansion coefficients. The high expansion coefficient of the *c*-axis ($52 \times 10^{-6}\,K^{-1}$) is in contrast to the fairly small values for *a*- and *b*-axis ($7 \times 10^{-6}\,K^{-1}$ and $2 \times 10^{-6}\,K^{-1}$), which result in the average value of $20.3 \times 10^{-6}\,K^{-1}$.
- In a strain hindered situation on the surface of an oxidic support the $V_2O_5$ particles cannot shrink without generating mismatch stresses.
- The analysis of the reflex width as a function of temperature shows small reflex width at the processing temperature and an increase for further cooling. Thus this alteration of the particle structure mainly occurs on cooling.
- The analysis of the peak width was used for a Williamson–Hall analysis. The active compound particles are both suffering residual stresses and they exhibit nano-structure of crystallites in the range of 20 nm.
- This could be confirmed by TEM. The high resolution images showed an interior nano-structure of differently oriented crystallites. Hence strain contours were detected near the interface.
- The peak width could be correlated to the activity of the catalyst. A mosaic structure of the $V_2O_5$-particles causes a higher activity most probably due to an increase in disordered locations. They are considered as additional active compounds.

## Acknowledgements

This work was subsidized by the German Research Foundation (Deutsche Forschungsgemeinschaft DFG) through the corporate research center "Structure, dynamics and reactivity of transition metal oxide aggregates" (Sonderforschungsbereich 546, project B7 with the help of B2 and B6, http://www.chemie.hu-berlin.de/sfb546).

## References

1. Beretta, A., Ranzi, E. and Forzatti, P., Production of olefins via oxidative dehydrogenation of light paraffins at short contact times. *Catal. Today*, 2001, **64**(1/2), 103–111.
2. Skarchenko, V. K., Oxidative dehydrogenation of hydrocarbons. *Russ. Chem. Rev.*, 1977, **46**(8), 731–748.
3. Sanfilippo, D. and Miracca, I., Dehydrogenation of paraffins: synergies between catalyst design and reactor engineering. *Catal. Today*, 2006, **111**(1/2), 133–139.
4. Buyanov, R. A. and Pakhomov, N. A., Catalysts and processes for paraffin and olefin dehydrogenation 1. *Kinet. Catal.*, 2001, **42**(1), 64–75.
5. Mars, P. and van Krevelen, D. W., Oxidations carried out by means of vanadium oxide catalysts. *Spec. Supp. Chem. Eng. Sci.*, 1954, **3**, 41–57.
6. Khodakov, A., Olthof, B., Bell, A. T. and Iglesia, E., Structure and catalytic properties of supported vanadium oxides: support effects on oxidative dehydrogenation reactions. *J. Catal.*, 1999, **181**(2), 205–216.
7. Arena, F., Frusteri, F. and Parmaliana, A., How oxide carriers affect the reactivity of $V_2O_5$ catalysts in the oxidative dehydrogenation of propane. *Catal. Lett.*, 1999, **60**(1/2), 59–63.
8. Lemonidou, A. A., Nalbandian, L. and Vasalos, I. A., Oxydative dehydrogenation of propane over vanadium oxide based catalysts: effects of support and alkali promoter. *Catal. Today*, 2000, **61**(1–4), 333–341.
9. Routray, K., Reddy, K. and Deo, G., Oxidative dehydrogenation of propane on $V_2O_5/Al_2O_3$ and $V_2O_5/TiO_2$ catalysts: understanding the effect of support by parameter estimation. *Appl. Catal. A*, 2004, **265**(1), 103–113.
10. Christodoulakis, A., Machli, M., Lemonidou, A. and Soghomon, B., Molecular structure and reactivity of vanadia-based catalysts for propane oxidative dehydrogenation studied by in situ Raman spectroscopy and catalytic activity measurements. *J. Catal.*, 2004, **222**(2), 293–306.
11. Besselmann, S., Freitag, C., Hinrichsen, O., Löffler, E. and Muhler, M., On the role of different vanadia species in the adsorption and oxidation

of toluene over $V_2O_5/TiO_2$ catalysts (Eurocat). In *Proc. 4th World Congr. Oxidat. Catal., vol. 1*, 2001, pp. 305–308.
12. Dias, C. R. and Portela, M. F., Synthesis of phtalic anhydride catalysts, kinetics and reaction modeling. *Catal. Rev. -Sci. Eng.*, 1997, **39**(3), 169–207.
13. Devriendt, K., Poelman, H. and Fiermans, L., The $V_2O_5/TiO_2$ (anatase) model catalyst structure: XPD study and single scattering cluster simulation. *Surf. Interf. Anal.*, 2000, **29**(2), 139–144.
14. Nogier, J. P. and Delamar, M., Investigations of the Eurocat $V_2O_5/TiO_2$ catalysts and of the $TiO_2$ support by secondary-ion mass spectrometry. *Catal. Today*, 1994, **20**(1), 125–134.
15. Silversmit, G., Poelman, H., Depla, D., Barrett, N., Marin, G. B. and De Gryse, R., A fully oxidized $V_2O_5/TiO_2$ (0 0 1)-anatase system studied with in situ synchrotron photoelectron spectroscopy. *Surf. Sci.*, 2005, **584**(2/3), 179–186.
16. Roozeboom, F., Mittelmeijer-Hazeleger, M. C., Moulijn, J. A., Medema, J., de Beer, V. H. J. and Gellings, P. J., Vanadium Oxide Monolayer catalysts. 3. A Raman spectroscopic and temperature-programmed reduction study of monolayer and crystal-type vanadia on various supports. *J. Phys. Chem.*, 1980, **84**(21), 2783–2791.
17. Rao, T. V. M. and Deo, G., Analysis of the kinetic parameters for the propane oxidative dehydrogenation reaction over $V_2O_5/Al_2O_3$ and $MoO_3/Al_2O_3$ catalysts. *AIChE*, 2007, **53**(5), 1538–1549.
18. Gao, X. and Wachs, I. E., Structural characteristics and reactivity properties of highly dispersed $Al_2O_3/SiO_2$ and $V_2O_5/Al_2O_3/SiO_2$ catalysts. *J. Catal.*, 2000, **192**(1), 18–28.
19. Bostan, A. I., Ilaposchenko, N. I., Pyatnitskii, Y. I., Raevskaya, L. N., Borisenko, M. V. and Dyachenko, A. G., Effect of the vanadium content in $V_2O_5/SiO_2$ catalysts on their activity and selectivity in the partial oxidation of methane. *Theor. Exp. Chem.*, 2002, **38**(5), 295–300.
20. Klisinska, A., Samson, K., Gressel, I. and Grzybowska, B., Effect of additives on properties of $V_2O_5/SiO_2$ and $V_2O_5/MgO$ catalysts. I. Oxidative dehydrogenation of propane and ethane. *Appl. Catal. A: Gen.*, 2006, **309**(1), 10–16.
21. Klisinska, A., Loridant, S., Grzybowska, B., Stoch, J. and Gressel, I., Effect of additives on properties of $V_2O_5/SiO_2$ and $V_2O_5/MgO$ catalysts. II. Physicochemical properties and structure of the catalysts and their correlations with oxidative dehydrogenation of propane and ethane. *Appl. Catal. A: Gen.*, 2006, **309**(1), 17–27.
22. Touloukian, Y. S., *Thermophysical Properties of Matter, Thermal Expansion*, *vol. 13*. Nonmetallic Solids, New York, 1977, p. 432.
23. Corvin, I. and Cartz, L., Anisotropic thermal expansion of $V_2O_5$. *J. Am. Ceram. Soc.*, 1965, **48**(6), 328–329.
24. Filatov, S. K., Anomale Wärmeausdehnung von $V_2O_5$. *Kristall Technik*, 1971, **6**(6), 777–785.
26. Warren, B. E., *X-Ray diffraction*. Dover Publications Inc., New York, 1969, p. 269.
27. Williamson, G. K. and Hall, W. H., X-ray line broadening from filed aluminium and wolfram. *Acta Metall.*, 1953, **1**(1), 22–31.
28. Nist database, http://www.ceramics.nist.gov/srd/summary/advmatdb.htm.